Inelastic Deuteron Scattering and (d,p) Reactions from Isotopes of Ti. V. Ti(d,d')†

P. WILHJELM AND OLE HANSEN
The Niels Bohr Institute, University of Copenhagen, Copenhagen, Denmark

AND

J. R. COMFORT, C. K. BOCKELMAN, AND P. D. BARNES
Yale University, New Haven, Connecticut

AND

A. SPERDUTO
Laboratory for Nuclear Science, Massachusetts Institute of Technology, Cambridge, Massachusetts

(Received 18 September 1967)

Results of elastic and inelastic deuteron scattering from ^{47,48,49,50}Ti are presented. Deuteron energies from 2.5 to 10 MeV were used, and (d,d') angular distributions were obtained at several energies in the ^{47,50}Ti cases. The elastic-scattering data are analyzed by means of the optical model, whereas the (d,d') data are analyzed in a simple direct-reaction picture employing collective-model-type form factors. The (d,d') data are in reasonable agreement with the direct-reaction predictions only at deuteron energies of 8 and 10 MeV. A reanalysis of the earlier Ti(d,p) results is presented. A deuteron potential in better agreement with the elastic-scattering data is used, resulting in an improved agreement with the (d,p) strength sum rules.

I. INTRODUCTION

IN previous papers we have reported results from experimental studies of Ti(d,p) reactions.[1] In the present paper, data from elastic and inelastic deuteron scattering from Ti isotopes are presented and discussed in terms of the optical model (elastic scattering) and a simple direct-reaction picture (inelastic-scattering data). A consistent description of the inelastic-deuteron-scattering results was not obtained with this model, probably indicating that more complicated mechanisms may be important. A reanalysis of the previous (d,p) results[1] is given. The reanalysis employs a deuteron optical potential found in the present Ti(d,d) analysis. This potential is similar to the potentials used in Ca(d,p) reactions[2] and to the ^{48}Ti(d,d) potentials of Siemssen and Böricke.[3]

II. EXPERIMENTAL PROCEDURES AND RESULTS

A. Elastic Scattering

The deuteron elastic-scattering experiments were performed in the 4.5-MV Van de Graaff Laboratory and in the 6.5-MV Tandem Accelerator Laboratory of the Niels Bohr Institute. The deuterons were detected by means of a surface-barrier counter and a 512-channel pulse-height analyser. Evaporated, enriched Ti targets on thin carbon backings were used. The targets contained Ta as an impurity.

At energies below 6 MeV the Ta(d,d) angular distributions follow the Rutherford expression. The ratio [(d,d) yield from Ti]/[(d,d) yield from Ta] was therefore taken as a measure of the ratio $(d\sigma_{el}/d\sigma_R)$, where $d\sigma_R/d\Omega$ designates the Rutherford cross section and $d\sigma_{el}/d\Omega$ the elastic-scattering cross section. At bombarding energies higher than 6 MeV the Ta(d,d) cross sections deviate from $d\sigma_R/d\Omega$, especially at back angles, and the Ti(d,d) yields were normalized (relatively) by the beam charge collected in the Faraday cup behind the thin target.

In the ^{47}Ti case the absolute-cross-section normalization was determined by assuming the $d\sigma_{el}/d\Omega$ to equal $d\sigma_R/d\Omega$ at 2.5 MeV and angles near 90° and at 3.0 MeV and angles near 60°. The angular distributions at both 2.5 and 3.0 MeV were (within experimental errors) identical to Rutherford scattering (see Fig. 1). ^{47}Ti angular distributions at other energies were normalized to the 3.0- and 2.5-MeV data by means of excitation functions measured at several angles.

In the ^{48}Ti case a small but systematic decrease of the elastic cross section relative to Rutherford scattering was observed at back angles at 2.5 and 3.0 MeV. The ^{48}Ti cross sections were therefore normalized at 2.5 MeV and forward angles to equal Rutherford scattering. If a procedure identical to the ^{47}Ti procedure had been followed, a cross-section scale about 8% higher would have resulted. The deviation from Rutherford scattering at back angles and 2.5- and 3-MeV bombarding energy is hardly outside the experimental errors.

^{49,50}Ti(d,d) angular distributions were measured at 6 MeV only. These yields were connected to the yields at 3.5 MeV and 45° by means of excitation functions.

† Work supported in part by the U. S. Atomic Energy Commission under Contract Nos. AT(30-1)3223 with Yale University and AT(30-1)2098 with M.I.T.

[1] P. D. Barnes, C. K. Bockelman, O. Hansen, and A. Sperduto, Phys. Rev. **136**, B438 (1964); **138**, B597 (1965); **140**, B42 (1965); P. D. Barnes, C. K. Bockelman, J. Comfort, O. Hansen, and A. Sperduto, *ibid.* **159**, 920 (1967).

[2] R. H. Bassel, R. M. Drisko, G. R. Satchler, L. L. Lee, J. P. Schiffer, and B. Zeidman, Phys. Rev. **136**, B960 (1964); **136**, B971 (1964).

[3] R. H. Siemssen and C. Mayer Böricke, Nucl. Phys. **A96**, 505 (1967).

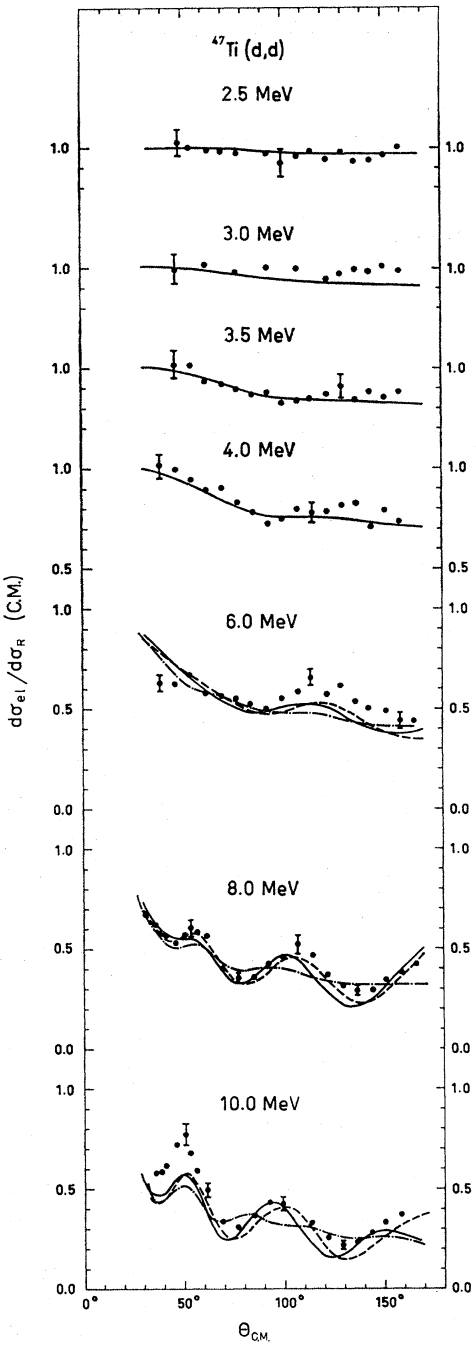

FIG. 1. Elastic scattering from ^{47}Ti. The experimental results are indicated by filled circles. Typical errors are shown by vertical bars. The observed cross sections are plotted relative to the Rutherford cross section. The full curves are optical-model fits obtained from potential CA of Table I. The dashed curves were generated from potential TI and the dot-and-dashed curves from potential B4.

The 3.5-MeV–45° cross sections were put equal to the average of ^{47}Ti and ^{48}Ti(d,d) cross sections at that energy and angle (95% of the Rutherford cross section).

It is believed that the over-all accuracy of the cross-section scales is better than ±22%. A relative error of ≈5% is ascribed to each measured yield.

The angular-distribution data are shown in Figs. 1 and 2.

B. Inelastic Scattering

The angular-distribution measurements at about 6 MeV were performed using the MIT-ONR electrostatic generator and the MIT multiangle heavy-particle spectrograph.[4]

The ^{47}Ti(d,d') data at $E_d=8$ and 10 MeV were measured by using the deuteron beam from the Copenhagen Tandem accelerator and a surface-barrier-detector arrangement. Two exposures were made in the heavy-particle spectrograph[5] at 45° lab angle and $E_d=8$ and 10 MeV, respectively. The high-resolution spectrograph data were used to make certain that the deuteron spectra observed with the counters had been correctly interpreted.

Measurements of the ^{47}Ti(d,d') reaction in the range 2.6–4.5 MeV were made with the deuteron beam from the Copenhagen 4.5-MV electrostatic generator. The scattered projectiles were detected in a heavy-particle spectrograph at an angle of 145° with respect to the beam. The procedures were nearly the same as those employed by Elbek in his Coulomb-excitation measurements.[6]

The cross-section scale was determined in each experiment by observing the ratio of inelastic- to elastic-scattering yield and by using the (d,d) cross sections of Sec. IIA. In each angular-distribution measurement the cross-section scale has been assigned an error of ±24%. Relative cross sections may be more accurate. The ^{47,49}Ti(d,d') data at 6 MeV, measured in the multigap spectrograph, are from the same exposures as the (d,p) reactions on these targets, and thus have cross-section scales deviating less than 15% from one another. The relative scales in the ^{50}Ti(d,d') data are also determined to within ±15%.

The data are presented in Figs. 3–6. It should be noted that the results shown in Fig. 6 were obtained at

TABLE I. Optical-model parameters.[a]

Potential	V (MeV)	r_0 (F)	a (F)	W' (MeV)	r_0' (F)	a' (F)	r_{0C} (F)
B4	103	1.00	0.90	25	1.41	0.65	1.30
CA	115	1.00	0.80	13	1.41	0.65	1.30
TI	112	1.00	0.80	13	1.41	0.65	1.00
TIL	115	1.00	0.80	24	1.41	0.65	1.00

[a] The form of the optical potential is given in the text.

[4] H. A. Enge and W. W. Buechner, Rev. Sci. Instr. 34, 155 (1963).

[5] J. Borggreen, B. Elbek, and L. Perch Nielsen, Nucl. Instr. Methods 24, 1 (1963).

[6] B. Elbek, *Determination of Nuclear Transition Probabilities by Coulomb Excitation* (Munksgaard, Copenhagen, 1963), and references cited therein.

slightly different lab angles. For $E_d \leq 4.5$ MeV, an angle of 145° was employed, whereas the 6-, 8-, and 10-MeV data were taken at angles from 142.5° to 150° (cf. the caption of Fig. 6).

III. ANALYSIS

A. Elastic Scattering

The observed elastic scattering was analyzed with an optical-model potential[7] of the form

$$U(r) = -V(1+\exp x)^{-1} + 4iW'(d/dx') \times (1+\exp x')^{-1} + V_C(r,r_C), \quad (1)$$

$$x = (r - r_0 A^{1/3})/a, \quad x' = (r - r_0' A^{1/3})/a';$$

and

$$r_C = r_{0C} A^{1/3}.$$

Fits to the observed elastic scattering were sought, starting from potentials known to give good accounts of (d,d), (d,d'), and (d,p) reactions in this mass region. No effort was made to obtain best fits or to investigate mass and energy dependence of the parameters in detail.

The potential B4 (Table I), used in our previous (d,p) analyses on Ti isotopes, gives a good account of the angular distributions at $E_d \leq 6$ MeV, but yields rather poor fits to the 8- and 10-MeV data on ^{47}Ti (see Fig. 1). A potential similar to the potentials used by Bassel *et al.*[2] (average-Z type potential) and by Belote *et al.*[8] in analyses of (d,d') and (d,p) reactions on Ca isotopes was found to give a satisfactory over-all account of the present data (potential CA of Table I). The fully drawn curves of Figs. 1 and 2 were obtained with this potential.

At $E_d = 6$, 8, and 10 MeV in the ^{47}Ti case the parameters were varied successively, starting from the CA potential, in order to see if small changes in the potential could bring about a better agreement between calculation and experiment. The very good fit at 8 MeV (potential TI) was obtained by lowering V by 3 MeV (and decreasing r_{0C}). The dashed curves in Fig. 1 were generated by this potential. No potential was found that would fully fit the 45° maximum at 10-MeV bombarding energy.

The dashed curve for ^{50}Ti(d,d) on Fig. 2 was calculated from potential TIL discussed below.

TABLE II. $(\beta_2 R)^2$ values for ^{50}Ti(1.55 MeV).

E_d (MeV)	Potential[a]	$(\beta_2 R)^2$	$B(E2)\uparrow/e^2$ (10^{-48} cm^4)	
5.5	CA	0.45		
6.0	CA	0.54		
6.5	CA	0.43		
Average	CA	0.47	0.026[b]	0.024±0.002[c]
5.5	TIL[d]	0.35		
6.0	TIL	0.51		
6.5	TIL[d]	0.54		
Average	TIL[d]	0.47	0.026[b]	0.024±0.002[c]

[a] Notation as in Table I.
[b] Calculated from $(\beta_2 R)^2$ by means of Eq. (3) of the text.
[c] Values from Coulomb excitation (Ref. 10).
[d] $W' = 22$ MeV at 6.5 MeV and 26 MeV at 5.5 MeV.

[7] An optical-model DW code written by J. Bang and P. Vedelsby was used. The code is similar to the inelastic-scattering option with collective form factors of code SALLY, originated by R. H. Bassel, R. M. Drisko, and G. R. Satchler. [See, e.g., Oak Ridge National Laboratory Report No. 3240, 1962 (unpublished).] The two codes give nearly identical results for Ti(d,d').

[8] T. A. Belote, J. H. Bjerregaard, O. Hansen, and G. R. Satchler, Phys. Rev. 138, B1067 (1965).

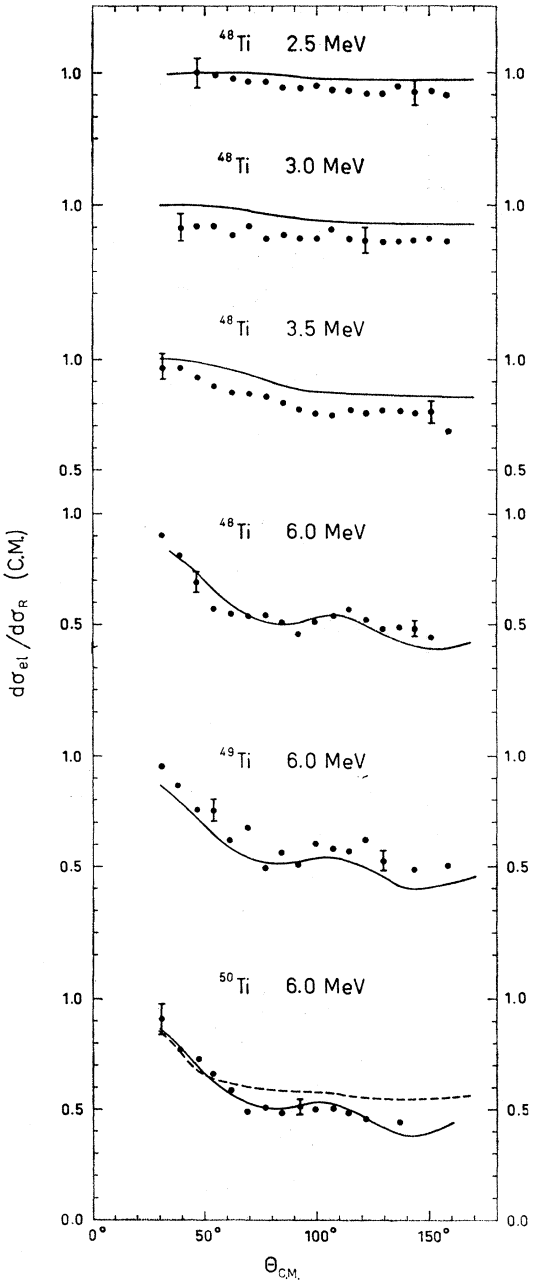

FIG. 2. Elastic scattering from ^{48}Ti, ^{49}Ti, and ^{50}Ti. The full curves are from potential CA and the dashed curve from potential TIL. The deviations at 2.5–3.5 MeV between prediction and results are inside the cross-section normalization uncertainty of the measurements.

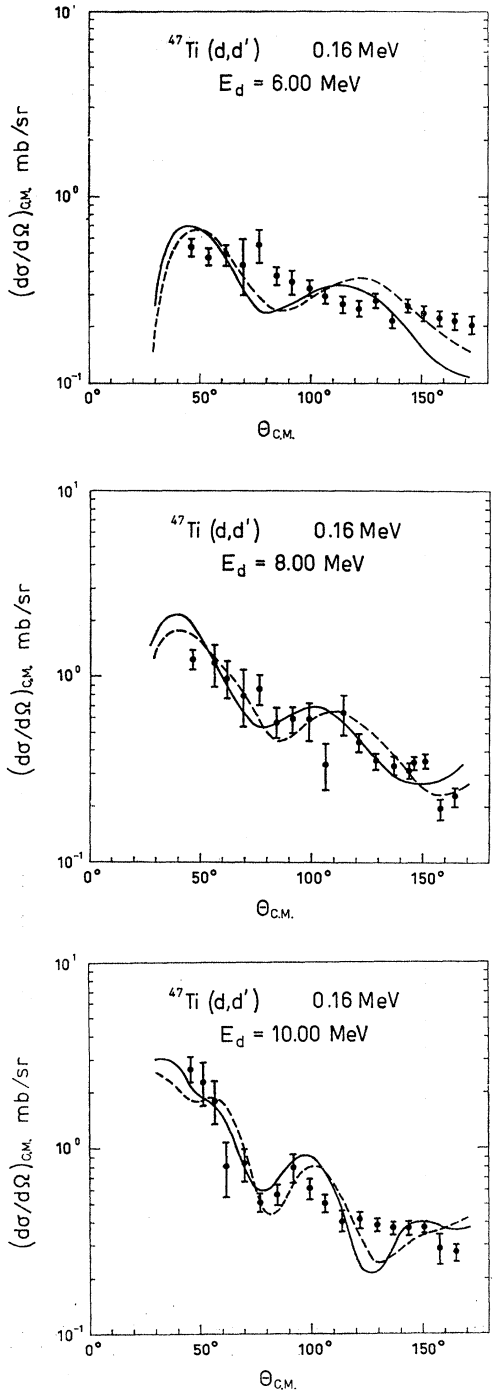

FIG. 3. ^{47}Ti(d,d') angular distributions. The full curves are DW fits, using potential CA; the dashed curves were generated using potential TI. The values of $(\beta_2 R)^2$ used for normalizing experiment and theory were 1.1, 1.8, and 2.0 at 6, 8, and 10 MeV, respectively.

B. Inelastic Scattering

The inelastic-scattering cross sections were analyzed by means of a distorted-wave (DW) code[7] with the use of a collective-model form factor ($l=2$) and complex coupling. Coulomb excitation was included.

The DW cross section is related to the experimental cross section by

$$(d\sigma/d\Omega)_{\text{expt}}=\frac{2J_f+1}{5(2J_i+1)}(\beta_2 R)^2(d\sigma/d\Omega)_{\text{DW}}. \quad (2)$$

TABLE III. ^{47}Ti (d,p) ^{48}Ti.[a]

Level No.	E_x (keV)	Strengths, B4 $l=1$	Strengths, B4 $l=3$	Strengths, CA $l=1$	Strengths, CA $l=3$
0	0	Nonstripping		Nonstripping	
1	983	···	2.05	···	1.20
2	2299	0.01	0.47	···	0.33
3	2423	0.17	···	0.13	···
4	3229	0.24	···	0.27	···
6	3342	0.02	0.62	···	0.58
8	3377	0.07	$\leqslant$0.07	0.06	$\leqslant$0.04
9	3520	?	0.41	?	(0.29)
10	3631	0.13	···	0.10	···
12	3752	0.03	0.35	(0.02)	(0.34)
15	4048	0.10	···	0.08	···
16	4087	0.05	···	0.04	···
17	4210	No l_n	···	No l_n	···
20	4403	0.61	···	0.46	···
21	4470	0.34	···	0.26	···
23–24	4595	Nonstripping		···	···
25	4734	0.18	···	0.14	···
27	4809	0.08	···	0.06	···
29	4876	0.14	···	0.11	···
30	4929	0.12	···	0.09	···
31	4956	0.08	···	0.06	···
33	5015	Nonstripping		···	···
34	5167	0.28	···	0.26	···
35	5271	Nonstripping		···	···
36	5319	No l_n	···	···	···
37	5398	0.04	0.19	0.03	0.18
38	5510	0.02	0.12	(0.01)	(0.08)
39	5537	No l_n	···	No l_n	···
40	5563	Nonstripping		···	···
41	5636	0.14	···	0.11	···
42	5652	0.55	···	0.44	···
43	5780	No l_n	···	No l_n	···
45	5906	0.21	···	0.17	···
46	6008	0.04	<0.09	$\approx$0.02	$\lesssim$0.10
47	6061	0.26	···	0.22	···
48	6136	No l_n	···	No l_n	···
49	6163	0.02	···	0.02	···
50	6332	0.24	···	0.20	···
51	6381	0.10	···	0.08	···
52	6509	0.04	0.55	0.04	0.42
53	6648	(0.03)	(0.13)	(0.03)	(0.11)
54	6701	0.15	0.37	0.11	0.46
55	6767	0.13	<0.09	0.11	<0.07
56	7250	0.07	<0.09	0.06	<0.08
57	7274	0.04	<0.09	0.03	<0.08
58	7377	0.18	···	0.16	···
59	7.45 MeV	0.15	···	0.13	···
60	7.50 MeV	No l_n	···	No l_n	···
61	7.58 MeV	No l_n	···	No l_n	···
62	7.73 MeV	0.08	0.17	No l_n	···
63	7.78 MeV	0.09	<0.08	0.08	<0.07
64	7.86 MeV	0.13	<0.07	0.11	<0.06
65	8.02 MeV	0.10	0.28	0.08	0.21
66	8.07 MeV	No l_n	···	No l_n	···
67	8.11 MeV	No l_n	···	No l_n	···

[a] Level numbering and excitation energies are identical to the previously published values (Ref. 1). Strength is here defined as $[(2J_f+1)/(2J_i+1)]\times S(J_i+j\rightarrow J_f)$. The B4 numbers for $l=3$ are thus $\frac{1}{4}$ of the previous numbers, whereas the $l=1$ strengths also have been corrected for a calculational error. The CA strengths were derived as explained in the text, and they represent a reinterpretation of the data.

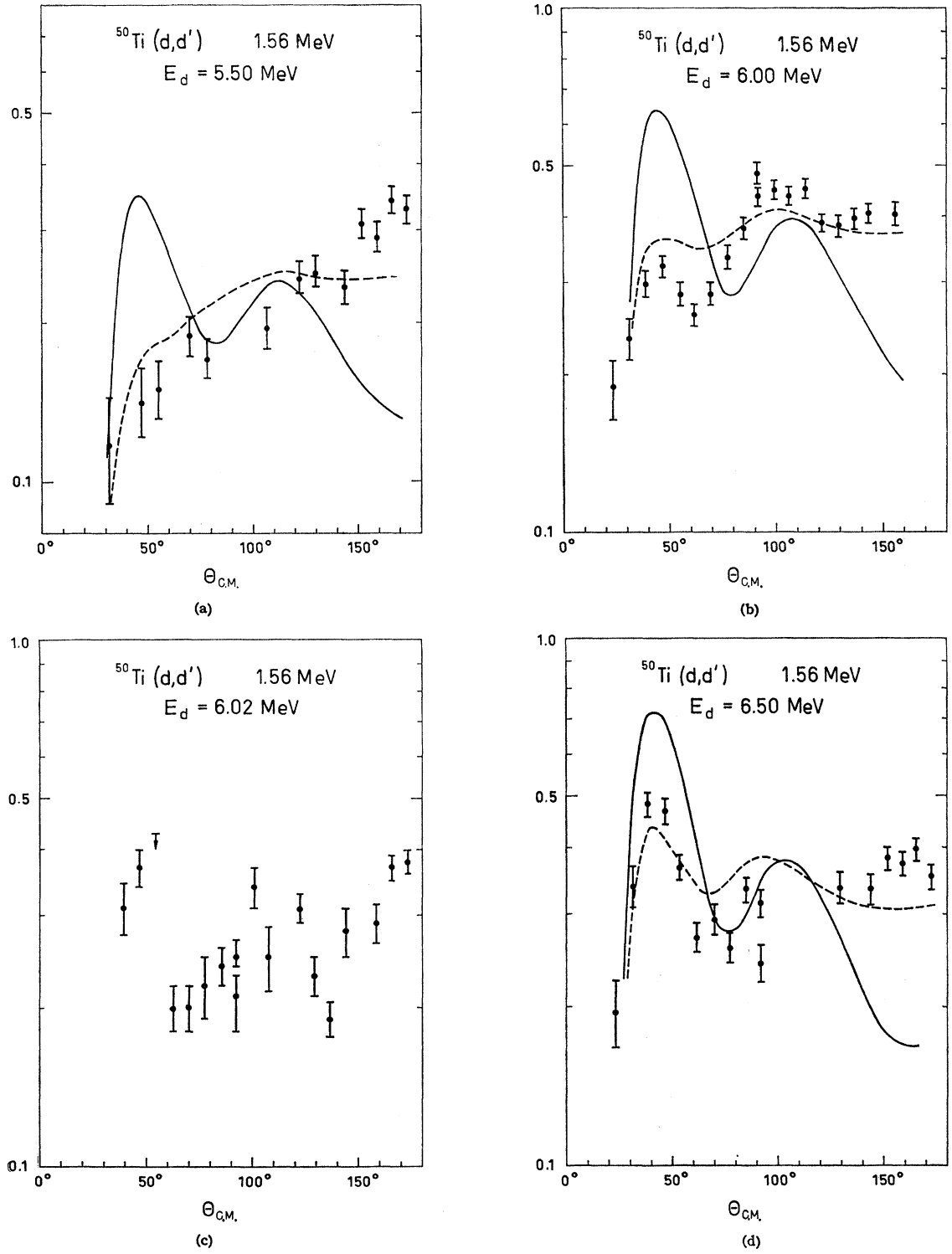

FIG. 4. ^{50}Ti(d,d') angular distributions. The full curves are DW fits using potential CA and the dashed curves were obtained from potential TIL. The $(\beta_2 R)^2$ values are given in Table II.

J_f and J_i are the final and initial spins, respectively. β_2 is the quadrupole deformability and $R=1.25A^{1/3}$ F. If the nucleus is homogeneously charged, $(\beta_2 R)^2$ is related to the reduced electric quadrupole transition

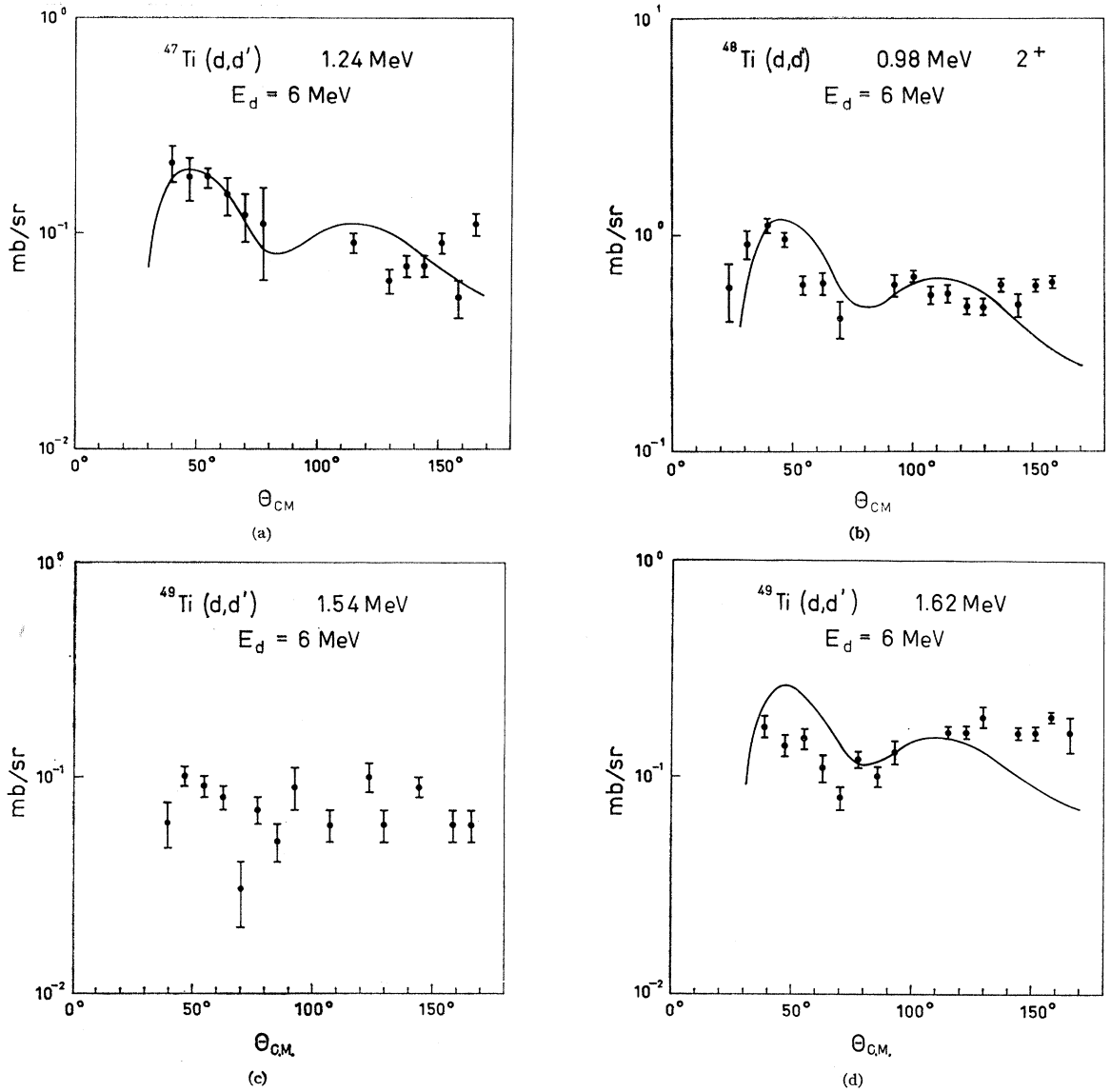

FIG. 5. (d,d') angular distributions from ^{47}Ti, ^{48}Ti, and ^{49}Ti. The states excited are marked by the excitation energy. The curves are DW predictions using potential CA and assuming an angular-momentum transfer of 2. $(\beta_2 R)^2$ values are given in the text.

probability $B(E2)\uparrow$ through

$$B(E2, J_i \rightarrow J_f)/e^2 = \left(\frac{3}{4\pi} ZR^2\right)^2 \beta_2^2 \frac{2J_f+1}{5(2J_i+1)}$$

$$\approx 560(\beta_2 R)^2[(2J_f+1)/5(2J_i+1)]\,\mathrm{F}^4 \quad (3)$$

using $Z=22$ and $A=47$.

1. $^{47}Ti(d,d')^{47}Ti$ (0.16 MeV)

The inelastic scattering to the 160-keV $\frac{7}{2}^-$ state of ^{47}Ti provides the case with the lowest energy loss and consequently also with the lowest momentum transfer studied here. Figure 3 shows the angular distributions generated from the CA and TI potentials (CA fully drawn and TI dashed). The over-all agreement between theory and experiment is reasonable, especially at the higher bombarding energies. The TI potential gives a somewhat better fit than the CA potential, as was also the case for elastic scattering.

Using the CA parameters, an excitation function was calculated for $\theta_{c.m.}=145°$. The predicted excitation function is shown in comparison with experiment in Fig. 6 applying a value of $(\beta_2 R)^2=1.2$, which is the mean of the $(\beta_2 R)^2$ values from the individual measurements. The over-all agreement between theory and experiment is not very good. Use of a constant potential yields a change in $(\beta_2 R)^2$ of a factor of 2 in going from

6 to 10 MeV bombarding energy. The TI potential gave a similar result.

From the 8- and 10-MeV data, we derive via Eq. (3) for $B(E2)\uparrow/e^2$ a value of 0.029×10^{-48} cm^4, as compared to a Coulomb-excitation value[9] of 0.028 in the same units. The data taken at $E_d\leq3$ MeV gives $B(E2)\uparrow/e^2=0.031$ when analyzed by the semiclassical first-order Coulomb-excitation theory and $B(E2)\uparrow/e^2\approx0.02$ from the DW analysis. We therefore conclude that the (d,d') process is reasonably described by the simple direct inelastic-scattering model only at $E_d\gtrsim8$ MeV.

TABLE IV. ^{48}Ti (d,p) ^{49}Ti.[a]

Level No.	E_x (keV)	l	Strength, B4	Strength, CA	Comments
0	0	3	3.0	2.13	
2	1384	1	2.4	1.87	
3	1544	...	...	...	
4	1587	1	0.08	0.06	
5	1625	...	...	...	
6	1724	1	0.56	0.45	
7	1762	...	...	...	
8	2261	...	...	...	
9	2472	...	...	...	
10	2503	0	0.07	0.05	2*s*
11	2517	3	0.89	0.70	
13	2665	...	...	...	
16	3042	...	...	...	
17	3176	1	0.37	0.31	
18	3261	(1)	(0.75)	(0.63)	
19	3430	(1)	(0.12)	(0.10)	
20	3469	1	0.05	0.04	
21	3517	...	...	...	
22	3610	...	...	...	
23	3639	...	...	...	
24	3699	...	...	...	
25	3749	...	...	...	
26	3787	1	0.30	0.26	
27	3844	(3)	(0.63)	(0.56)	
28	4075	...	...	...	
29	1443	...	...	...	
30	4195	...	...	...	
31	4222	1	0.14	0.12	
32	4360	...	...	...	
33	4434	1	0.15	0.13	
34	4456	...	...	...	
35	4505	(2)	(0.49)	(0.35)	2*d*
36	4588	1	0.10	0.09	
37	4667	(1)	(0.12)	(0.10)	
38	4770	(4)	(4.0)	(2.5)	
39	4836	...	...	...	
40	4897	2	0.39	0.29	
41	4911	...	...	...	
42	5063	...	...	...	
43	5120	...	...	...	
44	5173	...	...	...	
45	5253	(0)	(0.035)	(0.03)	
46	5326	...	...	...	
47	5375	...	...	...	
48	5412	(0)	(0.12)	(0.11)	
49	5437	1	0.06	0.05	
50	5579	...	...	...	
51	5655	...	...	...	
52	5693	(1)	(0.05)	(0.04)	
		(2)	(0.07)	(0.05)	
53	5737	1	0.11	0.10	

[a] Level numbering, excitation energies, and B4 strengths are identical to the numbers of Ref. 1.

[9] R. C. Ritter, P. H. Stelson, F. K. McGowan, and R. L. Robinson, Phys. Rev. **128**, 2320 (1962).

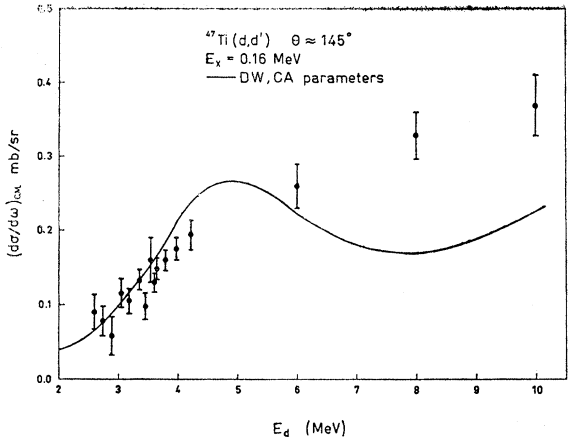

FIG. 6. ^{47}Ti(d,d') excitation function. The experimental points below 4.5 MeV were measured at $\theta_{lab}=145°$. The 6-MeV point was taken at $\theta_{lab}=142.5°$, whereas the 8- and 10-MeV points were obtained at 150°. It appears from the angular-distribution data (Fig. 5) that the cross section changes but slowly around 145°. The curve was obtained from DW calculations using the CA parameters and $(\beta_2R)^2=1.2$.

An effort to restore agreement by letting the d potential vary with bombarding energy is described below for the case of ^{50}Ti(d,d').

2. $^{50}Ti(d,d')^{50}Ti$ (1.55 MeV)

The ^{50}Ti(d,d') reaction to the 1.55-MeV 2^+ state is subject to one of the largest energy losses and consequently one of the largest momentum transfers studied here.

The calculated angular distributions at 5.5, 6.0, and 6.5 MeV, using the CA parameters (fully drawn curves), are shown in comparison with the data in Fig. 4. The agreement between theory and experiment is poor. The rapid change of the shape of the angular distributions with bombarding energy is not reproduced.

The dashed curves were obtained by increasing the absorptive potentials by almost a factor of 2 and by allowing W' to vary with bombarding energy. The 6-MeV curve is from potential TIL, the 5.5-MeV curve from a potential with $W'=26$ MeV, and the 6.5-MeV curve has $W'=22$ MeV. In this way the gross structure of the shapes may be reproduced but only at the expense of the agreement with elastic scattering (Fig. 2, ^{50}Ti, dashed curve). The change in (d,d') angular-distribution shape from 6.00 to 6.02 MeV is not reproduced.

The values of $(\beta_2R)^2$ obtained from the CA and TIL parameters are given in Table II, in comparison with the Coulomb-excitation $B(E2)\uparrow$ value.[10] In view of the difficulties encountered in fitting the measured cross sections one should probably not give too much attention to the excellent agreement between Coulomb excitation and (d,d') data in this case.

[10] J. Simpson, J. Cookson, D. Eccleshall, and M. Yates, Nucl. Phys. **62**, 385 (1965).

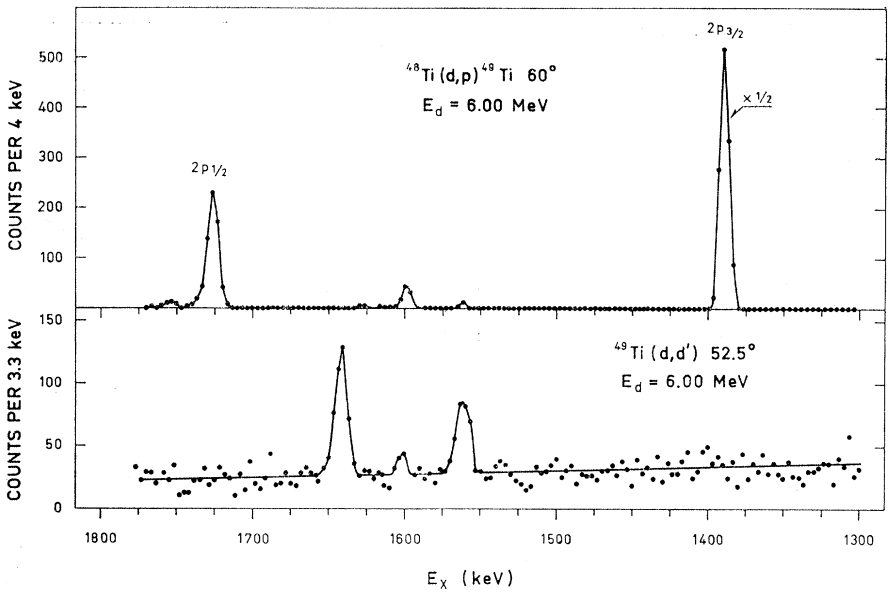

FIG. 7. Comparison of ^{48}Ti-(d,p) and ^{49}Ti(d,d') spectra. The (d,p) data are from Ref. 1. The figure illustrates that the two reactions excite different states in ^{49}Ti.

The rapid change in angular-distribution shape near 6 MeV would seem in qualitative disagreement with a simple direct mechanism and points to possible compound effects.

3. *Miscellaneous Ti(d,d') Reactions*

The ^{48}Ti(d,d') transition to the 0.98-MeV 2^+ state has a forward-peaked shape and is reasonably well fitted by a DW curve using the CA parameters (Fig. 5). $(\beta_2 R)^2=0.67$, the equivalent $B(E2)$ being 0.04 $\times 10^{-48}$ cm^4. The Coulomb-excitation and lifetime-measurement values[11] give $(0.07\pm0.014)\times10^{-48}$ cm^4.

The 1.24-MeV state of ^{47}Ti is rather strongly excited in the (d,d') reaction with a value $[\text{of } (2J_f+1)/5(2J_i+1)](\beta_2 R)^2=0.13$ (CA parameters). The spin of this state is not known. In the ^{46}Ti(d,p) reaction[12] the transition to the 1.24-MeV state is weak and of nonstripping character.

In the ^{49}Ti(d,d') reaction only the transitions to the states at 1.62 and 1.54 MeV were strong enough to permit angular-distribution measurements. The shapes as observed (Fig. 5) are rather uncharacteristic and do not agree well with the DW predictions (CA parameters). Values of $[(2J_f+1)/5(2J_i+1)](\beta_2 R)^2$ of 0.23 (1.62 MeV) and 0.11 (1.54 MeV) were obtained.

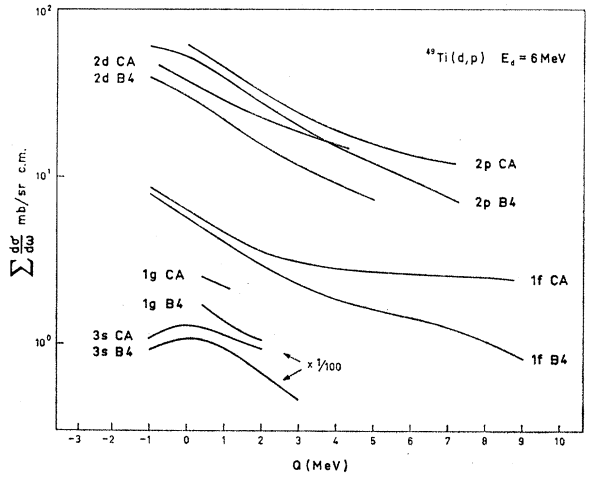

FIG. 8. Summed DW cross sections versus Q value. The calculated cross sections were summed over the center-of-mass angles employed in the (d,p) experiments, i.e., from laboratory angles of $\theta=7.5°$ to $\theta=165°$ in steps of 7.5°. The deuteron potentials and shell-model orbits used are indicated at each curve. These curves were used for interpolating in Q between the sample calculations.

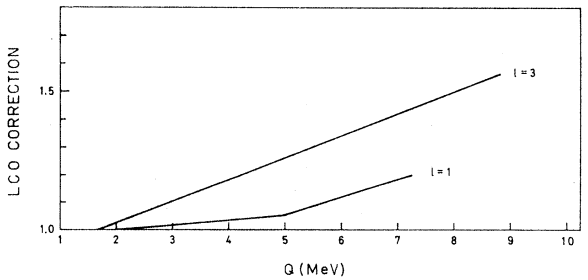

FIG. 9. The ratio $f=\sigma_{DW}(\text{LCO}=0)/\frac{1}{2}[\sigma_{DW}(\text{LCO}=0)+\sigma_{DW}(\text{LCO}=4.5\text{ F})]$ is plotted versus Q values. LCO stands for lower cutoff radius. Spectroscopic strengths were extracted from the measured cross sections by means of the LCO=0 calculations, and were subsequently multiplied by the ratio f. (Also see the text.)

[11] P. H. Stelson and L. Grodzins, Nucl. Data **1A**, 21 (1965).
[12] J. Rapaport, A. Sperduto, and W. W. Buechner, Phys. Rev. 143, 808 (1966).

TABLE V. ^{49}Ti (d,p) ^{50}Ti.[a]

Level No.	E_x (keV)	Strengths, B4 $l=1$	$l=3$	$l=0$	$l=2$	$l=4$	Strengths, CA $l=1$	$l=3$	$l=0$	$l=2$	$l=4$	Comments
0	0	···	1.41	···	···	···	···	0.76	···	···	···	
1	1555	0.12	0.44	···	···	···	0.08	0.32	···	···	···	
2	2686	0.06	···	···	···	···	0.04	$\leqslant$0.01	···	···	···	
3	3208	Nonstripping		···	···	···	···	···	···	···	···	
5	3879	Nonstripping		···	···	···	···	···	···	···	···	
6	4158	0.91	···	···	···	···	0.74	···	···	···	···	
7	4184	1.14	···	···	···	···	0.93	···	···	···	···	
8	4322	0.03	···	···	···	···	0.02	···	···	···	···	
9	4422	···	···	0.004	0.014	···	···	···	0.003	0.009	···	3s, 2d
10	4536	No l_n	···	···	···	···	No l_n	···	···	···	···	
11	4576	No l_n	···	···	···	···	No l_n	···	···	···	···	
13	4808	0.06	···	···	···	···	0.05	···	···	···	···	
14	4898	1.0	···	···	···	···	0.81	···	···	···	···	
17	5203	0.25	···	···	···	···	0.20	···	···	···	···	
18	5348	Nonstripping		···	···	···	···	···	···	···	···	
19	5395	0.28	···	···	···	···	0.23	···	···	···	···	
20	5440	0.01	0.05	···	···	···	0.01	0.06	···	···	···	
21	5561	0.03	···	···	···	···	0.03	···	···	···	···	
22	5600	0.015	0.08	···	···	···	0.01	0.08	···	···	···	
24	5717	Nonstripping		···	···	···	···	···	···	···	···	
25	5821	0.004	0.10	···	···	···	0.004	0.08	···	···	···	
26	5851	0.02	0.15	···	···	···	0.02	0.13	···	···	···	
27	5956	0.35	···	···	···	···	0.29	···	···	···	···	
29	6079	0.02	···	···	···	···	0.02	···	···	···	···	
30	6138	0.19	0.48	···	···	···	0.15	0.50	···	···	···	
31	6176	0.03	···	···	···	···	0.02	···	···	···	···	
32	6210	···	···	···	(0.06)	···	···	···	···	(0.04)	···	2d
33	6250	0.006	0.16	···	···	···	No l_n	···	···	···	···	
34	6325	No l_n	···	···	···	···	No l_n	···	···	···	···	
35	6392	0.08	···	···	···	···	0.07	···	···	···	···	
37	6498	0.04	···	···	···	···	0.04	···	···	···	···	
38	6536	0.12	0.44	···	···	···	0.09	0.47	···	···	···	
39	6592	No l_n	···	···	···	···	No l_n	···	···	···	···	
40	6636	···	0.30	···	···	···	···	0.26	···	···	···	
41	6697	Nonstripping		···	···	···	···	···	···	···	···	
42	6726	0.29	···	···	···	···	0.25	···	···	···	···	
43	6744	···	···	0.02	···	···	···	···	0.01	···	···	3s
44	6863	0.14	0.24	···	···	···	0.09	0.41	···	···	···	
45	6913	Nonstripping		···	···	···	···	···	···	···	···	
46	6986	Nonstripping		···	···	···	···	···	···	···	···	
47	7025	0.06	···	···	···	···	0.05	···	···	···	···	
48	7049	0.035	···	···	···	···	0.03	···	···	···	···	
49	7094	···	···	···	0.04	···	···	···	···	0.03	···	2d
50	7132	···	···	···	0.07	···	···	···	···	0.05	···	2d
51	7178	···	0.19	···	···	···	···	0.17	···	···	···	
52	7229	0.02	···	···	···	···	0.02	···	···	···	···	
53	7249	0.10	···	···	···	···	0.09	···	···	···	···	
54	7280	···	0.02	···	···	···	···	0.01	···	···	···	
55	7387	···	···	···	0.01	0.83	···	···	···	$\approx$0.005	0.56	2d, 1g
56	7407	0.03	···	···	···	···	0.02	···	···	···	···	
57	7447	No l_n	···	···	···	···	No l_n	···	···	···	···	
58	7471	0.05	···	···	···	···	0.04	···	···	···	···	
59	7504	0.12	0.16	···	···	···	0.09	0.13	···	···	···	
60	7550	0.03	0.26	···	···	···	No l_n	···	···	···	···	
61	7631	0.10	···	···	···	···	0.09	···	···	···	···	
62	7663	···	0.91[b]	···	···	···	···	0.80[b]	···	···	···	

[a] Level numbers and excitation energies are unchanged from Ref. 1. Strengths are defined as in Table III and thus the B4 $l=3$ and $l=4$ strengths here are $\frac{1}{2}$ of those previously published. The B4, $l=1$, and $l=2$ strengths have been corrected for calculational mistakes. The CA strengths represent a reinterpretation of the data.

[b] Could also be fitted with $l_n=2+4$.

Figure 7 shows part of a ^{49}Ti(d,d') spectrum in comparison with the corresponding section of a ^{48}Ti(d,p) spectrum.[1] The two strong (d,d') transitions correspond to nonstripping transitions, and the strong (d,p), single-particle transitions correspond to states weakly excited in the (d,d') reaction. Qualitatively the data

TABLE VI. ^{50}Ti (d,p) ^{51}Ti.[a]

Level No.	E_x (keV)	l	Strength, B4	Strength, CA	Comments
0	0	1	3.07	2.46	
1	1160	1	1.16	0.96	
2	1429	...	...	...	
3	1559	...	...	...	
4	2136	3	2.36	2.01	
5	2189	1	0.30	0.26	
6	2896	1	0.72	0.62	
7	3164	1	0.41	0.35	
8	3759	4	5.39	3.7	
9	4012	(3)[b]	(0.34)	(0.31)	
10	4162	(2)[b]	(0.36)	(0.29)	2*d*
11	4460	...	...	...	
12	4559	1	0.12	0.10	
13	4592	(2)[b]	(0.65)	(0.53)	2*d*
14	4747	...	...	...	
15	4810	0	0.11	0.09	3*s*
16	4872	0	0.15	0.13	3*s*
17	4988	(0)	(0.10)	0.08	3*s*
18	5003				
19	5092	...	...	...	
20	5139	3	2.41	2.17	
21	5214	...	...	...	

[a] Level numbering and excitation energies are unchanged from Ref. 1. B4 strengths for $l=1$ have been corrected.
[b] $l=1$ is not excluded definitely.

are consistent with the (d,d') reaction, exciting mainly collective states, i.e., states of strongly mixed configurations. Quantitatively, a consistent description of the (d,d') data has not been found, probably reflecting the oversimplified assumptions about the reaction mechanism underlying the DW analysis.

IV. REANALYSIS OF THE (d,p) RESULTS

The above analysis of ^{47}Ti(d,d) and the ^{48}Ti(d,d) analysis of Ref. 3 indicate that a deuteron potential with a smaller absorption than used in the previous (d,p) analyses[1] (potential B4) should be considered. DW calculations using the CA potential indicate that the cross sections for the high-Q-value (d,p) transitions are changed by almost a factor of 2 relative to the cross sections generated by the B4 potential. The complete (d,p) data of Ref. 1 were therefore reanalyzed using the CA potential. With its smaller absorption this potential generates (d,p) cross sections that are more sensitive to the value of the lower cutoff radius than was the case for the B4 potential. The summed differential DW cross sections for potentials B4 and CA are shown in Fig. 8 plotted versus the Q value. The proton potential of Ref. 1 was used; a lower cutoff radius of zero and no spin-orbit coupling were employed. Generally, the CA potential leads to larger cross sections than does the B4 potential, especially at high Q values. The fits obtained for the CA potential are similar to those obtained with the B4 potential, though the predictions differ at the highest Q values ($Q\gtrsim 7$ MeV) and at very forward angles.

The factor

$$f=\sigma_{\mathrm{DW}}(\mathrm{LCO}=0)/\tfrac{1}{2}[\sigma_{\mathrm{DW}}(\mathrm{LCO}=0)+\sigma_{\mathrm{DW}}(\mathrm{LCO}=4.5\ \mathrm{F})],$$

where LCO stands for lower cutoff radius, is plotted versus Q in Fig. 9. The spectroscopic strengths obtained from experiment by means of the LCO=0 calculations were multiplied by this factor (cf. the discussions in Refs. 2 and 13). The procedures outlined previously[1] were otherwise followed when extracting spectroscopic information from the data. The influence of including a spin-orbit term in the bound-state potential of 25 times the Thomas value was investigated. For $l=3$, cross-section changes of $\approx 10\%$ were encountered; for $l=1$ the changes were $\lesssim 5\%$.

The B4 curves of Fig. 8 differ from the earlier ones[1] for $l=1$ and 2, since two trivial calculational errors were found during the analysis. Tables III–VI present the new strengths for potential B4 and for potential CA. In the latter case, we have generally been more conservative in the l assignments than previously. The values in Tables III–VI supersede the spectroscopic strengths of Ref. 1.

The strength sums are collected in Table VII, and it is seen that the CA analysis gives values in better agreement with the sum rules than the B4 calculations.

TABLE VII. (d,p)-sum-rule analysis.[a]

Target	Shell-model orbit	Strength sum, B4	Strength sum, CA	Theory
^{47}Ti	$1f_{7/2}$	3.9	2.8	3
	$2p$	5.5	4.4	6
	$1f_{5/2}$	1.8	1.5	6
^{48}Ti	$1f_{7/2}$	3.0	2.1	2
	$2p$	5.3	4.3	6
	$1f_{5/2}$	1.5	1.3	6
	$2d_{5/2}$	0.9	0.6	6
	$3s_{1/2}$	0.15	0.1	2
	$1g_{9/2}$	4.0	2.5	10
	$2s_{1/2}$	0.07	0.05	0
^{49}Ti	$1f_{7/2}$	1.85	1.1	1
	$2p$	5.7	4.6	6
	$1f_{5/2}$	3.5	3.1	6
	$2d_{5/2}$	0.2	0.1	6
	$3s_{1/2}$	0.02	0.01	2
	$1g_{9/2}$	0.8	0.6	10
^{50}Ti	$1f_{7/2}$	0	0	0
	$2p$	5.8	4.8	6
	$1f_{5/2}$	5.1	4.5	6
	$2d_{5/2}$	1.0	0.8	6
	$3s_{1/2}$	0.4	0.3	2
	$1g_{9/2}$	5.4	3.7	10

[a] The shell-model assignments are identical to those argued in the previous papers (Ref. 1). The theoretical strengths are derived assuming pure $f_{7/2}$ ground states. The experimental error of $\pm 24\%$ in the absolute cross sections must also be applied to the experimental strength sums.

[13] J. H. Bjerregaard, O. Hansen, and G. Sidenius, Phys. Rev. **138**, B1097 (1965); M. de Lopez, M. Mazari, W. Dorenbusch, T. A. Belote, and O. Hansen, Nucl. Phys. **A94**, 673 (1967); J. H. Bjerregaard and O. Hansen, Phys. Rev. **155**, 1229 (1967).

Also, the systematic overfulfillment of the sum rules has disappeared. The CA strengths are generally just outside the experimental uncertainties assigned to the earlier strengths.

It is of interest to note that the need for an $l=0$ contribution in the ^{47}Ti$(d,p)^{48}$Ti transition to the first 6^+ state (No. 6 in Table III) has disappeared. Since the ^{47}Ti ground-state spin is $\frac{5}{2}$, such an admixture is not allowed, so the argument that a doublet may exist here, is no longer valid.

ACKNOWLEDGMENTS

We are indebted to Mrs. Bonnie Andersen, Mrs. Virginia Camp, Mrs. K. Sakamoto, Mrs. M. Nagatani, Mrs. Mieko Kitajima, and Mrs. Carmen Vanegas for carefully scanning the nuclear track plates. The cooperation of the NBI-NORDITA GIER computer center and the help of Dr. J. H. Bjerregaard, Mrs. L. Vistisen, and Mrs. B. Scharff in the (d,p) reanalysis are gratefully acknowledged.

PHYSICAL REVIEW VOLUME 166, NUMBER 4 20 FEBRUARY 1968

Nuclear Spin, Hyperfine-Structure Separation, and Nuclear Magnetic Moment of 18-min ^{88}Rb†

PAUL A. VANDEN BOUT,* ANTONI DYMANUS,‡ VERNON J. EHLERS,§ MICHAEL H. PRIOR, AND HOWARD A. SHUGART

Department of Physics and Lawrence Radiation Laboratory, University of California, Berkeley, California

(Received 8 September 1967)

We have used the atomic-beam magnetic-resonance technique to measure the nuclear spin and the hyperfine-structure separation of 18-min ^{88}Rb in the $^2S_{1/2}$ electronic ground state. These results, combined with the Fermi-Segrè formula, yield the nuclear magnetic moment. Our results are: $I=2$, $\Delta\nu=\pm1186.084(18)$ MHz, $\mu_I(\text{uncorr})=\pm0.506(5)$ nm, $\mu_I(\text{corr})=\pm0.508(5)$ nm. Present nuclear theory favors assignment of the negative sign to the value of the moment.

I. INTRODUCTION

DEVELOPMENT of nuclear theories has in the past depended heavily upon the experimental measurement of static nuclear properties, and in particular upon the determination of nuclear spins and multipole moments. Although several nuclear theories are now reasonably well established, such information still serves as a useful guide in the further development of these theories, and allows determination of the ground state of the nuclei involved. As part of our continuing program to measure pertinent nuclear properties, we have measured the nuclear spin, hyperfine-structure separation, and nuclear magnetic moment of ^{88}Rb.

Two features of ^{88}Rb make it of special interest. First, it is an odd-odd nucleus, and a measurement of its spin and magnetic moment serves as a good check on various proposed coupling schemes for odd-odd nuclei. Second, it is the heaviest in a series of eight Rb isotopes for which the spins and magnetic moments have been measured. The change in nuclear properties caused by the one-by-one addition of neutrons is particularly amenable to comparison with nuclear theories, and thus it is desirable to measure the nuclear properties of a chain of isotopes.

† Research supported by the U. S. Atomic Energy Commission.

* Present address: Columbia University, Physics Department, New York, N. Y.

‡ On leave from University of Nijmegen, Netherlands.

§ Present address: Calvin College, Grand Rapids, Mich.

II. THEORY OF THE EXPERIMENT

The Hamiltonian describing the hyperfine structure (hfs) of ^{88}Rb is given by

$$\mathcal{H}=ha\mathbf{I}\cdot\mathbf{J}-g_J\mu_0\mathbf{J}\cdot\mathbf{H}-g_I\mu_0\mathbf{I}\cdot\mathbf{H}, \quad (1)$$

where a is the magnetic-dipole hfs interaction constant, $\mathbf{I}h$ is the nuclear angular momentum, $\mathbf{J}h$ is the electronic angular momentum, $g_I=\mu_I/I$ and $g_J=\mu_J/J$ are the corresponding g factors, $\mathbf{H}$ is the external magnetic field, h is Planck's constant, and μ_0 is the Bohr magneton. The energy levels of Eq. (1) for $J=\frac{1}{2}$ are given by the Breit-Rabi formula,

$$W(F,M_F)=\frac{-h\Delta\nu}{2(2I+1)}-g_I\mu_0HM_F+(F-I)h\Delta\nu\{1+4M_Fx/(2I+1)+x^2\}^{1/2}, \quad (2)$$

where $\Delta\nu=a(I+\frac{1}{2})$, $x=(g_I-g_J)(\mu_0/h)H/\Delta\nu$, and $\mathbf{F}=\mathbf{I}+\mathbf{J}$. These levels are illustrated in Fig. 1 for ^{88}Rb.

The theory of operation of an atomic-beam apparatus has been described in detail elsewhere[1]; we give only a brief sketch here. Atoms effuse from the slit of an oven at one end of an evacuated chamber and pass through three magnetic fields. The first is strongly inhomogeneous and the atoms suffer deflections due to their mag-

[1] N. F. Ramsey, *Molecular Beams* (Oxford University Press, New York, 1956).